Advances in Applied Mathematics and Mechanics
Adv. Appl. Math. Mech., Vol. **4**, No. 1, pp. 72-92

DOI: 10.4208/aamm.11-m1160
February 2012

A Consistent Characteristic Boundary Condition for General Fluid Mixture and Its Implementation in a Preconditioning Scheme

Hua-Guang Li[1,3], Nan Zong[2], Xi-Yun Lu[1] and Vigor Yang[3,*]

[1] *Department of Modern Mechanics, The University of Science and Technology of China, Hefei, Anhui 230026, China*
[2] *Department of Mechanical and Nuclear Engineering, The Pennsylvania State University, University Park, PA 16802, USA*
[3] *School of Aerospace Engineering, The Georgia Institute of Technology, Atlanta, GA 30332, USA*

Received 23 March 2011; Accepted (in revised version) 21 June 2011

Available online 13 December 2011

Abstract. Characteristic boundary conditions that are capable of handling general fluid mixtures flow at all flow speeds are developed. The formulation is based on fundamental thermodynamics theories incorporated into an efficient preconditioning scheme in a unified manner. Local one-dimensional inviscid (LODI) relations compatible to the preconditioning system are proposed to obtain information carried by incoming characteristic waves at boundaries accurately. The approach has been validated against a variety of sample problems at a broad range of fluid states and flow speeds. Both acoustic waves and hydrodynamic flow features can pass through the boundaries of computational domain transparently without any unphysical reflection or spurious distortion. The approach can be reliably applied to fluid flows at extensive thermodynamic states and flow speeds in numerical simulations. Moreover, the use of the boundary condition shows to improve the computational efficiency.

AMS subject classifications: 65M10, 78A48

Key words: Real-fluid, preconditioning method, method of characteristics, LODI relations.

1 Introduction

Proper implementation of boundary conditions is of great importance in obtaining reliable and accurate numerical solutions of compressible flows. Much effort has been

*Corresponding author.
URL: `http://soliton.ae.gatech.edu/people/vigor.yang/`
Email: lhg@mail.ustc.edu.cn (H. G. Li), zongnan@gmail.com (N. Zong), xlu@ustc.edu.cn (X. Y. Lu), vigor.yang@aerospace.gatech.edu (V. Yang)

applied to develop robust numerical boundary conditions based on the method of characteristics (MOC) [1]. The technology was originated from the classical characteristic solution of differential equations of a hyperbolic system [2]. The MOC method was later extended to address multidimensional inviscid system with non-reflective acoustic boundary conditions [3]. Poinsot and Lele [4] further developed an approach capable of treating viscous compressible flows. They derived local one-dimensional inviscid (LODI) relations to calculate quantities associated with incoming characteristic waves and improved the accuracy of the method. The viscous terms are added separately and can be relaxed smoothly to inviscid flows as viscous effects diminish. Except for problems with gently varying flow and weak acoustic wave near boundaries, the boundary conditions based on characteristic method can usually get more accurate and physical results than simple extrapolation method or simplified Riemann invariants boundary conditions. In addition, the method gives rise to a more robust solution procedure. Baum et al. [5] extended the characteristic boundary conditions from equations which only can consider perfect gas with constant homogeneous thermodynamic properties to accommodate multi-component reactive flows with variable thermodynamic properties. Although the characteristic boundary conditions have been widely used, most of those studies, however, focused on treating the fluid flows in the ideal gas regime. Very limited work has been conducted to develop a consistent boundary treatment for fluid flows under high-pressure and low-temperature conditions, for which the method based on ideal gas does not work and real fluids effects must be considered [6].

Many fluid flows involve thermodynamic states in the trans-critical and supercritical regimes, where the real-fluid effect is notably strong. Fluid properties may experience severe variations when approaching the liquid-gas critical point [7] (see Fig. 3). This is important in heat transfer and fluid dynamics and raises a challenge to the boundary condition treatment. For example, a very small thermal disturbance can generate enormous unsteadiness in the form of shock and expansion waves in a near-critical fluid due to the abnormally high fluid compressibility, a phenomenon known as the piston-effect in near-critical fluids [7]. The boundary conditions must be treated properly to avoid unphysical oscillations and reflections that will then propagate into the computational domain and ruin the solution. Okong'o and Bellan [8] extended MOC based boundary conditions from ideal gas to multi-component real-fluid mixtures. The formulations have been validated against the convection of a single vortex in supercritical heptane/nitrogen homogeneous mixture with supersonic flow speeds. Although it has been demonstrated that the extended characteristic boundary condition can successfully treat fluid flows with moderate real-fluid effects in high-speed flow regimes, the method cannot be directly implemented to handle transcritical or supercritical fluid flows at very low flow speeds because there is no low Mach number flow treatment technique such as the preconditioning method [9–11].

In this paper, we aim at developing consistent boundary conditions for general fluid mixtures flow at all speeds. The acoustic wave propagation related formulations, such as system eigenvalues and eigenvectors, are derived based on the unified

treatment of general fluid thermodynamics [6, 14] and incorporated into an efficient preconditioning scheme [11] to deal with low Mach number flows. The LODI relations were proposed for the governing system with preconditioning techniques in a consistent manner.

The feasibility and robustness of the method are examined through testing cases with a broad range of fluid state and flow speed. The acoustic wave propagation case shows the method with real-fluid effects treatment works well at the ideal gas regime. The single vortex convection case demonstrates the capability of handling real-fluid flow with Mach number ranging from 0.1 to 1.6. The near-critical fluid piston effect case shows the current method works well even when fluid properties exhibit anomalies. It is also shown that the implementation of this consistent boundary condition results in a fast convergence in the pseudo-time space and thus enhances the computational efficiency.

This paper is organized as follows. In Section 2, theoretical framework is described, including the improved preconditioning schemes [11] and formulation derivation for the characteristic boundary conditions. Section 3 introduces numerical implementation and carries out numerical tests. Finally a brief summary concludes the present work.

2 Theoretical formulation

2.1 Euler equations and preconditioning scheme

To facilitate discussion, only the three-dimensional preconditioned Euler equations with species equations are considered. The viscous terms can be approached separately as introduced by Poinsot and Lele [4]. The preconditioned conservation equations used here exhibit the following form,

$$\Gamma\frac{\partial\widehat{Q}}{\partial\tau}+\frac{\partial Q}{\partial t}+\frac{\partial E}{\partial x}+\frac{\partial F}{\partial y}+\frac{\partial G}{\partial z}=0, \tag{2.1}$$

where Γ represents the preconditioning matrix and τ the pseudo-time. The conservative variable vector, Q is defined as

$$Q=\left(\rho,\rho u,\rho v,\rho w,\rho e_t,\rho Y_1,\rho Y_2,\cdots,\rho Y_{N-1}\right)^T. \tag{2.2}$$

Pressure-temperature type of primitive variables is adopted as the independent variables. The pseudo-time variable vector, $\widehat{Q}$ is defined as,

$$\widehat{Q}=\left(p',u,v,w,T,Y_1,Y_2,\cdots,Y_{N-1}\right)^T, \tag{2.3}$$

where ρ denotes the density, u,v and w the velocity components. T and e_t denote the temperature and the specific total energy, respectively. Y_i and N denote the mass

fraction of species i and the number of species, respectively. Explicit expressions of the convective flux vectors E, F and G are given by Hsieh and Yang [10], Meng and Yang [6] and Oefelein [15]. The pressure p is decomposed into a constant reference pressure p_0 and gauge pressure p' to circumvent the pressure singularity problem at low Mach numbers [9],

$$p = p_0 + p'. \tag{2.4}$$

The details of this method can be found in [11].

2.2 Method of characteristics

The method of characteristics is introduced by transforming the governing equations to characteristic form. Define Jacobian matrices as

$$T = \frac{\partial Q}{\partial \widehat{Q}}, \qquad A = \frac{\partial E}{\partial \widehat{Q}}, \qquad B = \frac{\partial F}{\partial \widehat{Q}}, \qquad C = \frac{\partial G}{\partial \widehat{Q}}, \tag{2.5}$$

then Eq. (2.1) can be written as

$$\Gamma \frac{\partial \widehat{Q}}{\partial \tau} + T \frac{\partial \widehat{Q}}{\partial t} + A \frac{\partial \widehat{Q}}{\partial x} + B \frac{\partial \widehat{Q}}{\partial y} + C \frac{\partial \widehat{Q}}{\partial z} = 0. \tag{2.6}$$

The eigen-properties of the preconditioning system are determined by the matrix $\Gamma^{-1}A$, $\Gamma^{-1}B$ and $\Gamma^{-1}C$ instead of A, B and C for Navier-Stokes equations. For brevity, only operation in the x-direction is discussed. Characteristic form of the preconditioning system (2.1) can be obtained through diagonalizing $\Gamma^{-1}A$

$$\Gamma^{-1}A = M \Lambda M^{-1}, \tag{2.7}$$

where the columns of M consist of eigenvectors of $\Gamma^{-1}A$, and diagonal components of Λ consist of the eigenvalues of $\Gamma^{-1}A$. The matrix Γ and A are given in the appendix. Due to involving both preconditioning process and real-fluid effects, the derivation is more complex than that for ideal gas. With a series of matrix operation, M and Λ can be obtained. Here we give the matrix in a way convenient for developing code,

$$M = \begin{bmatrix} M_{11} & M_{21} & 0 & 0 & 0 & 0 & \cdots & 0 \\ M_{12} & M_{22} & 0 & 0 & 0 & 0 & \cdots & 0 \\ 0 & 0 & 1 & 0 & 0 & 0 & \cdots & 0 \\ 0 & 0 & 0 & 1 & 0 & 0 & \cdots & 0 \\ 1 & 1 & 0 & 0 & 1 & 0 & \cdots & 0 \\ 0 & 0 & 0 & 0 & 0 & 1 & \cdots & 0 \\ \vdots & \vdots & \vdots & \vdots & \vdots & \vdots & \ddots & \vdots \\ 0 & 0 & 0 & 0 & 0 & 0 & \cdots & 1 \end{bmatrix}. \tag{2.8}$$

The components of matrix M are given by

$$M_{11} = \frac{A_T \gamma p + B_T \rho^2 a^2}{\gamma \rho R_0}, \qquad M_{12} = M_{11},$$
$$M_{21} = \frac{R_1(R_2+R_3)}{\rho R_0(\gamma^{1/2}R_4 - \gamma R_3 u/\Theta + \gamma R_3 u a^2)}, \quad M_{22} = \frac{R_1(R_2-R_3)}{\rho R_0(\gamma^{1/2}R_4 + \gamma R_3 u/\Theta - \gamma R_3 u a^2)},$$

where a, γ and Θ represent the sound speed, the specific heat ratio and the scaling factor, respectively,

$$\Theta = \frac{\varepsilon^{-2} + (\gamma - 1)}{a^2},$$

and ε is a preconditioning factor that can optimally control the convection and diffusion process [9, 12, 13]. Optimal values are specified locally by the relation

$$\varepsilon = \min\left\{1, \max\{\varepsilon_{inv}, \varepsilon_{\Delta t}, \varepsilon_{vis}\}\right\}.$$

The subscripts inv, Δt, and vis refer to the inviscid, unsteady, and viscous preconditioning factors, respectively

$$\varepsilon_{inv} = \begin{cases} \varepsilon_0^2, & M \le \varepsilon_0, \\ 2M^2, & \varepsilon < M < 1, \\ 1, & M \ge 1. \end{cases}$$

The term ε_0 is a small number and is included to avoid singularities in stagnation regions where $M = 0$

$$\varepsilon_{\Delta t} = \frac{1}{a^2}\left[\left(\frac{l_x}{\pi \Delta t}\right) + \left(\frac{l_y}{\pi \Delta t}\right) + \left(\frac{l_z}{\pi \Delta t}\right)\right] + M^2.$$

Here, l_x, l_y and l_z represent the characteristic dimensions of the computational domain and M is the Mach number

$$\varepsilon_{vis} = \left[\frac{\tilde{u}^2 \delta_x(\delta_x - 1)}{\tilde{u}^2 \delta_x^2 + a^2}, \frac{\tilde{v}^2 \delta_y(\delta_y - 1)}{\tilde{v}^2 \delta_y^2 + a^2}, \frac{\tilde{w}^2 \delta_z(\delta_z - 1)}{\tilde{w}^2 \delta_z^2 + a^2}\right],$$

and

$$\delta_x = \frac{\nu}{u}\frac{CFL}{VNN}, \qquad \delta_y = \frac{\nu}{v}\frac{CFL}{VNN}, \qquad \delta_z = \frac{\nu}{w}\frac{CFL}{VNN},$$

where ν is viscous coefficient. The parameters

$$A_T = \left(\frac{\partial p}{\partial T}\right)_{\rho_i}, \qquad B_T = \left(\frac{\partial e}{\partial T}\right)_{p, Y_i},$$

can be derived from basic thermodynamics relations [11]. The parameters R_i are given by

$$R_0 = \sum_{i=1}^{N} Y_i \widehat{e}_i - e - \frac{p}{\rho}, \qquad R_1 = B_T\rho^2 a^2 + A_T\gamma\Big(pa^2 + \frac{\gamma}{\Theta}\rho R_0\Big),$$
$$R_2 = 2\gamma^{\frac{1}{2}}u(1+\varepsilon)R_1, \qquad R_3 = 2R_1((1-\varepsilon)^2\gamma u^2 + 4\gamma\varepsilon a^2)^{\frac{1}{2}},$$
$$R_4 = 2B_T\rho^2 a^6 + \frac{\gamma^3}{\Theta^2}B_T\rho^2 a^2 u^2 - 2\frac{\gamma}{\Theta}B_T\rho^2 a^4 u^2 + B_T\gamma\rho^2 a^6 u^2$$
$$+ A_T\gamma^2\Big(pa^4u^2 + 2\frac{\gamma}{\Theta}B_T pa^2(a^2-u^2) + \frac{\gamma^2}{\Theta^2}(2\rho a^2 R_0 + \gamma p u^2)\Big),$$

where $\widehat{e}_i$ is the partial-density internal energy [6],

$$\widehat{e}_i = \Big(\frac{\partial\rho e}{\partial\rho_i}\Big)_{T,\rho_{j\neq i}}. \tag{2.9}$$

The inverse of matrix M is given as

$$M^{-1} = \begin{bmatrix} M'_{11} & M'_{12} & 0 & 0 & 0 & 0 & \cdots & 0 \\ M'_{21} & M'_{22} & 0 & 0 & 0 & 0 & \cdots & 0 \\ 0 & 0 & 1 & 0 & 0 & 0 & \cdots & 0 \\ 0 & 0 & 0 & 1 & 0 & 0 & \cdots & 0 \\ M'_{51} & 0 & 0 & 0 & 1 & 0 & \cdots & 0 \\ 0 & 0 & 0 & 0 & 0 & 1 & \cdots & 0 \\ \vdots & \vdots & \vdots & \vdots & \vdots & \vdots & \ddots & \vdots \\ 0 & 0 & 0 & 0 & 0 & 0 & \cdots & 1 \end{bmatrix}, \tag{2.10}$$

where

$$M'_{11} = \frac{M_{22}}{M_{11}M_{22} - M_{12}M_{21}}, \quad M'_{12} = \frac{M_{12}}{M_{11}M_{22} - M_{12}M_{21}}, \quad M'_{21} = \frac{M_{21}}{M_{11}M_{22} - M_{12}M_{21}},$$
$$M'_{22} = \frac{M_{11}}{M_{11}M_{22} - M_{12}M_{21}}, \quad M'_{51} = \frac{M_{21} - M_{22}}{M_{11}M_{22} - M_{12}M_{21}}.$$

The diagonal eigenvalue matrix Λ is

$$\Lambda = diag(\ \lambda_1 \quad \lambda_2 \quad \cdots \quad \lambda_{N+3} \quad \lambda_{N+4}\ ), \tag{2.11}$$

where λ_1 and λ_2 represent the rescaled acoustic wave speed propagating upstream and downstream, respectively,

$$\lambda_1 = \frac{1}{2}\Big[(1+\varepsilon)u - \sqrt{(1-\varepsilon)^2u^2 + 4\varepsilon a^2}\Big], \tag{2.12a}$$
$$\lambda_2 = \frac{1}{2}\Big[(1+\varepsilon)u + \sqrt{(1-\varepsilon)^2u^2 + 4\varepsilon a^2}\Big], \tag{2.12b}$$
$$\lambda_{3\sim N+4} = u. \tag{2.12c}$$

All of the eigenvalues in the pseudo-time space are real and have signs consistent with the directions of characteristic wave propagation. The present scheme not only preserves the hyperbolicity of the system, but also gives rise to individual eigenvalues that behave in a manner representative of the physical reality involved [10].

Eq. (2.1) is placed in characteristic form through multiplying by $M^{-1}\Gamma^{-1}$,

$$M^{-1}\Gamma^{-1}\Big(\Gamma\frac{\partial\widehat{Q}}{\partial\tau}+\mathrm{T}\frac{\partial\widehat{Q}}{\partial t}+A\frac{\partial\widehat{Q}}{\partial x}+B\frac{\partial\widehat{Q}}{\partial y}+C\frac{\partial\widehat{Q}}{\partial z}\Big)=0. \tag{2.13}$$

To simplify Eq. (2.13), define variables D and V as

$$D\equiv\Gamma^{-1}\Big(\mathrm{T}\frac{\partial\widehat{Q}}{\partial t}+B\frac{\partial\widehat{Q}}{\partial y}+C\frac{\partial\widehat{Q}}{\partial z}\Big), \tag{2.14a}$$

$$dV\equiv M^{-1}d\widehat{Q}+M^{-1}Dd\tau. \tag{2.14b}$$

Eq. (2.13) then can be written into characteristic form in terms of V,

$$\frac{\partial V}{\partial\tau}+\Lambda\frac{\partial V}{\partial x}=0, \tag{2.15}$$

or

$$\frac{\partial V}{\partial\tau}+L=0, \tag{2.16}$$

where

$$L=\big(L_1,L_2,\cdots,L_{N+3},L_{N+4}\big)^T=\Lambda\frac{\partial V}{\partial x}. \tag{2.17}$$

The propagating direction of characteristic waves is determined by the sign of the characteristic values (λ_i). The variables V and L corresponding to outgoing waves must be specified from solution of interior computational domain, and those corresponding to incoming waves must be determined from information of exterior computational domain.

2.3 Local one-dimensional inviscid relations

LODI relations are introduced to avoid arbitrariness in deciding information from exterior computational domain. Since conservation form of the governing equations is usually preferred in a compressible flow simulation, Eq. (2.15) is written into a more applicable form,

$$\Gamma\frac{\partial\widehat{Q}}{\partial\tau}+\mathrm{T}\frac{\partial\widehat{Q}}{\partial t}=-\Big(B\frac{\partial\widehat{Q}}{\partial y}+C\frac{\partial\widehat{Q}}{\partial z}\Big)-\Gamma ML. \tag{2.18}$$

By neglecting the transverse convective term and viscous term, LODI relations can be derived for the preconditioning system,

$$\Gamma\frac{\partial\widehat{Q}}{\partial\tau}+\mathrm{T}\frac{\partial\widehat{Q}}{\partial t}+\Gamma ML=0. \tag{2.19}$$

Considering that the pseudo-time term will converge to zero, Eq. (2.19) becomes

$$\frac{\partial Q}{\partial t} + \Gamma ML = 0. \tag{2.20}$$

The application of the LODI relations is in the same way as that introduced by Poinsot and Lele [4]. First solve L_i corresponding to outgoing characteristic waves from inside computational domain solution, then solve the rest L_i through LODI relations, and finally, substitute L_i into Eq. (2.18) and solve it to obtain all independent quantities at boundaries.

3 Treatments of various boundary conditions

3.1 Subsonic outflow boundary conditions

For simplicity and not losing generality, we take $u > 0$, $\lambda_1 < 0$ and $\lambda_2 > 0$ for subsonic outflow boundary condition. The sign of the eigenvalues indicates the propagating direction of characteristic waves. There are $N+3$ outgoing and one incoming characteristic waves at the boundary. For the outgoing waves associated with $\lambda_{2\sim N+4}$, $L_{2\sim N+4}$ can be obtained from solution of inside computational domain. For the incoming wave associated with λ_1, we can solve L_1 through LODI relations to get partial reflecting boundary condition, or set $L_1 = 0$ to get perfectly non-reflecting boundary condition. However, simply setting $L_1 = 0$ will raise pressure drifting which could become a serious problem in the calculation. Rudy and Strikerda [16], Poisot and Lele [4], and Baum et al. [5] have proposed that for the incoming wave on subsonic outflow boundary,

$$L_1 = k(p - p_\infty), \tag{3.1}$$

should be used to feedback information of infinite field pressure p_∞ into the computational domain, where k is a factor to determine the speed with which the average pressure in the computational domain relaxes towards the imposed pressure at infinity. Rudy and Strikerda [16] proposed that optimal value of k is given by

$$k = \frac{2\sigma\varepsilon a^2(1 - \mathrm{M}^2)}{l_c\sqrt{u(1-\varepsilon)^2 + 4\varepsilon a^2}}, \tag{3.2}$$

where M represents the maximum Mach number in the computational domain, l_c is the characteristic length of the domain and σ is a scaling factor for optimization. Substitute L_i into Eq. (2.18) and solve it combining with equation of state, and then we can obtain all independent physical quantities at the outflow boundary.

3.2 Subsonic inflow boundary conditions

For subsonic inflow boundary conditions we still take $u > 0$, $\lambda_1 < 0$ and $\lambda_2 > 0$. Accordingly, there are $N+3$ incoming and one outgoing characteristic waves on the subsonic inflow boundary. Many physical conditions can be applied to subsonic inflow

boundary. Here we choose to give u, v, w, T and Y_i for the inlet boundary condition. L_1 can be obtained from solution of inside computational domain, and then $L_{2\sim N+4}$ can be solved through LODI relations. With the given boundary conditions and solved L_i, we can solve the first equation in Eq. (2.18) combining with equation of state to obtain gauge pressure p' and finally get all independent quantities on the inlet boundary.

3.3 Supersonic outflow boundary conditions

For supersonic outflow boundary conditions with $u > 0$, $\lambda_1 > 0$ and $\lambda_2 > 0$, all characteristic waves on the boundary are outgoing. Therefore, all L_i can be obtained from inside computational domain solution and no additional boundary condition is required.

3.4 Supersonic inflow boundary conditions

For supersonic inflow boundary conditions with $u > 0$, $\lambda_1 > 0$ and $\lambda_2 > 0$, all characteristic waves are incoming, so all independent quantities p, u, v, w, T and Y_i should be given on this boundary.

4 Numerical method

A dual-time-stepping integration technique is implemented to obtain time-accurate results [6, 10, 14, 17]. The solution converged in pseudo-time corresponds to a time-accurate solution in physical time. One major advantage of this technique lies in the fact that the convergence of the iterative process is dictated by the well-behaved eigenvalues in the pseudo-time space, instead of the original eigenvalues that may become disparate in certain flow regimes (e.g., low Mach number flows [17]). A standard fourth-order Runge-Kutta scheme is employed to perform the inner-loop pseudo-time integration because of its relatively higher temporal accuracy and greater stability margin compared to many commonly used explicit schemes [18]. A local pseudo-time step is used to accelerate the convergence. To obtain an accurate result, a convergence criterion requires that relative residual error decreases three orders at least and is smaller than 10^{-5}. The temporal discretization of the real-time derivative term is obtained using a second-order backward difference. Spatial discretization is achieved by means of a fourth-order flux-differencing scheme [19]. Further improvement is acquired by adding both the second- and fourth-order artificial dissipation with a total-variation-diminish (TVD) switch [20,21] to ensure numerical stability and convergence. The second-order artificial dissipation term is enforced only in regions with strong gradients, whereas the fourth-order term is applied in smooth regimes to achieve numerical stability. For boundary conditions, the same time integration scheme as interior field is used and one-sided third-order difference scheme is used for special discretization.

5 Test cases

Three problems have been tackled to demonstrate the validity and capability of the present method, including one-dimensional acoustic wave propagation in the mixture of nitrogen and oxygen at standard state, one-dimensional piston effect in nitrogen with pressure at the critical point $p_0 = p_{cr}$ and temperature slightly above the critical point $T_0 = T_{cr} + 0.1$K, and two-dimensional single vortex convection in high-pressure cryogenic nitrogen/oxygen mixture with a compressibility factor of 0.4. The widely used modified Soave-Redlich-Kwong (SRK) equation of state is adopted for the first and third samples to realize the treatment of real fluids [22]. Benedict-Webb-Rubin (BWR) equation of state is adopted for the near-critical nitrogen piston effect case because it is more accurate than the SRK equation of state to handle the anomalies exhibited by fluid properties in the close vicinity of the liquid-gas critical point [23]. However, the computational cost of the BWR equation is larger than that of the SRK equation, and the latter is as accurate as the former in the regimes except for near-critical and liquid regimes. To exhibit the flexibility of the present method, the two equations of state are used for different cases.

5.1 One-dimensional acoustic wave propagation in ideal gas mixture

One purpose of the non-reflecting MOC boundary condition is to eliminate non-physical reflection of acoustic waves penetrating an outflow boundary. Accordingly, the case of one-dimensional acoustic waves propagating towards an outflow boundary is often used to test boundary condition methods. Similar to Baum's work [5], the one-dimensional acoustic wave is given as follows. The velocity distribution is

$$u = u_0 + b \exp\Big[- \Big(c \frac{x - 0.5l}{l} \Big)^2 \Big]. \tag{5.1}$$

The pressure distribution is

$$p = p_0 + p' = p_0 + \rho_0 a_0 (u - u_0). \tag{5.2}$$

The density distribution is

$$\rho = \rho_0 + \frac{\rho_0 (u - u_0)}{a_0}. \tag{5.3}$$

The mass fractions are

$$Y_{O_2} = 0.33, \qquad Y_{N_2} = 0.67. \tag{5.4}$$

The domain length l measures 1m. The reference velocity u_0 is 1m/s. The reference pressure p_0 is 1atm. The reference density ρ_0 is 1.18kg/m^3 . The parameter b and c, taking value of 10 and 5, determine the strength and stiffness of the acoustic wave, respectively.

Fig. 1 shows the process of the acoustic wave propagating towards the outflow boundary. The acoustic wave passed through the outflow boundary smoothly without

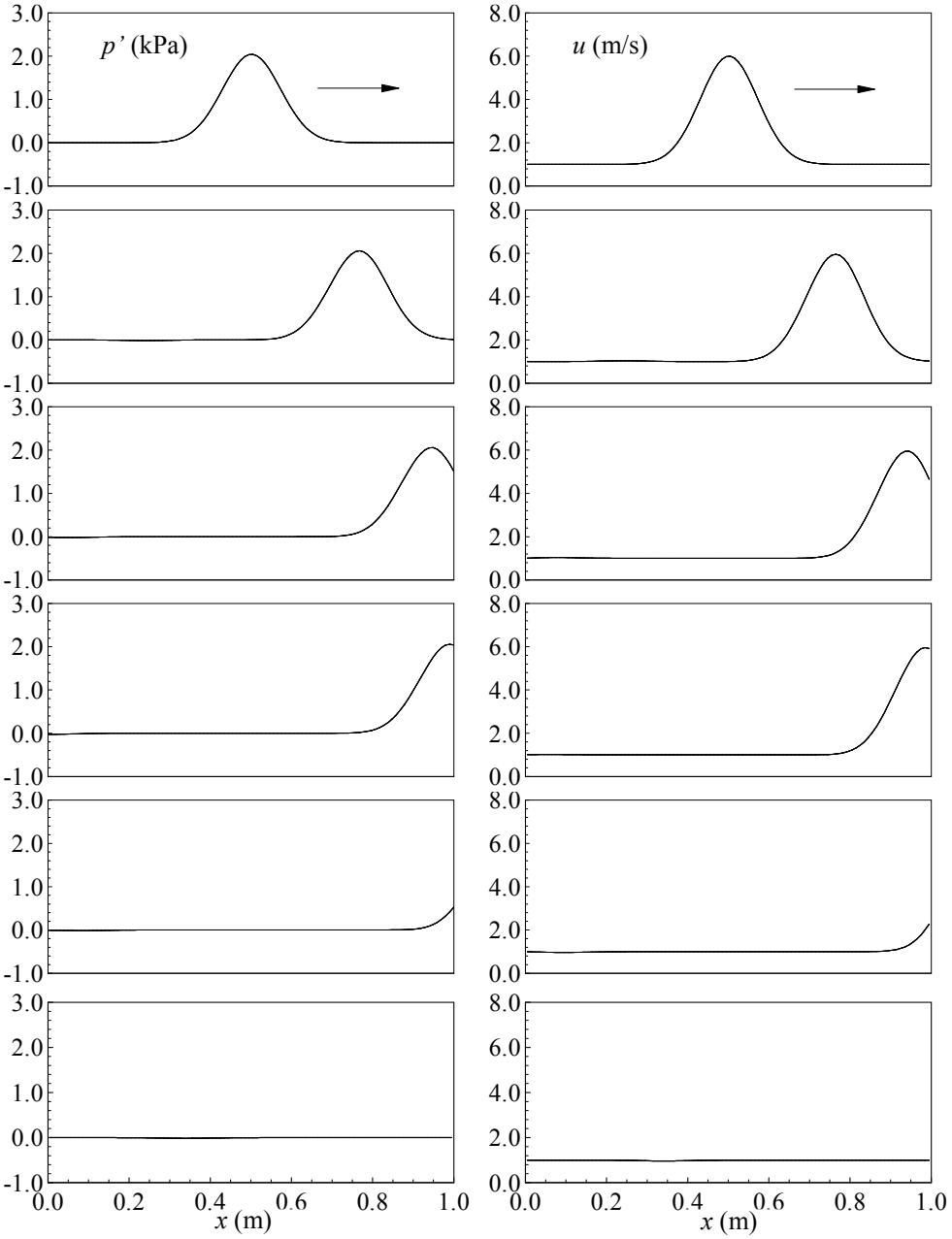

Figure 1: Propagation of acoustic wave towards outflow boundary at $x = 1$m in ideal-gas mixture with an interval 0.3ms: gauge pressure p' (left column) and velocity u (right column).

noticeable disturbance. More accurately, two probes are set at two positions, $x/l = 0.8$ and the outflow boundary, to record the local pressure and velocity variation through time. As shown in Fig. 2, both the strength and stiffness of the acoustic wave are kept well without noticeable change during the entire propagation process. This also demonstrates that the current method can relax to ideal gas regime smoothly.

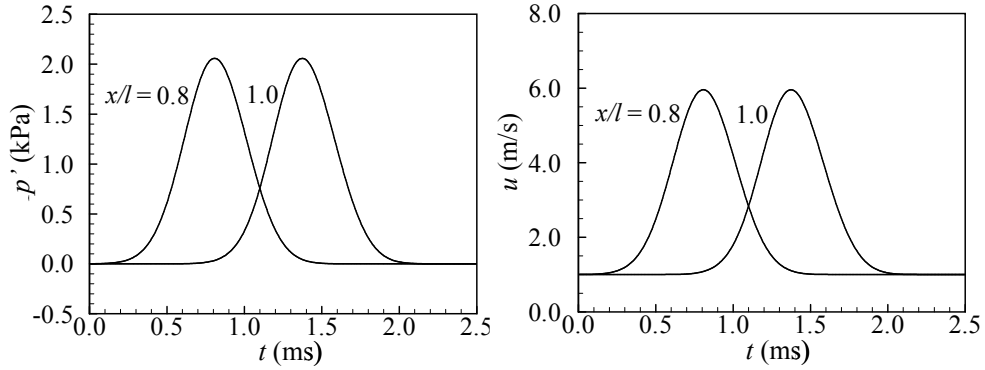

Figure 2: Propagation of the acoustic wave recorded by probes at $x = 0.8$m and outflow boundary $x = 1$m: gauge pressure (left) and velocity (right).

5.2 One-dimensional piston effect in near-critical nitrogen

To examine the performance of the current boundary treatment in the fluid regime with strong real-fluid effects, the piston effect induced by thermal heating at the boundary of a near-critical fluid is modeled. The thermodynamic and transport anomalies occur when temperature and pressure approach the liquid-gas critical point (shown in Fig. 3). Under such a condition, the coefficient of volume expansion and isothermal compressibility approach infinite. And consequently, a very small change of temperature/pressure of a near-critical fluid can lead to a significant volume dilatation. For instance, a more than 50 percent density reduction of nitrogen fluid occurs when temperature increases about one Kelvin from the critical value, whereas a one Kelvin temperature increasing can only induce less than 0.5% of density variation at the standard state. In addition, the heat capacity under constant pressure diverges and thermal diffusivity tends to be zero in the regime close to the critical point. For instance, the thermal diffusion of near-critical nitrogen at $(T_{cr} + 1\text{K}, p_{cr})$ is more than three orders of magnitude lower than that under standard state conditions, which makes the conduction process extremely slow in a near-critical fluid. The highly variable properties of near-critical fluid have substantial impact in aspects of fluid dynamic and heat transfer.

The piston effect is the response of a compressible fluid to a thermal disturbance. For example, in compressible fluids, a hot thermal boundary generated near a heated wall expands in acoustic time scale and acts like a piston. If the thermal disturbance is strong and rapid enough, shock waves could be generated. For the highly compressible and low thermal diffusive near-critical fluid, this effect becomes prominent, and anomalous heat transport by the piston effect happens [7]. Accurate and consistent boundary conditions are needed to deal with the strong real-fluid effects and strong acoustic waves. Moreover, the preconditioning method is suitable to handle the large disparity between acoustic time scale, flow time scale and diffusion time scale in this case. BWR equation of state is used to calculate the highly variable thermodynamic properties accurately.

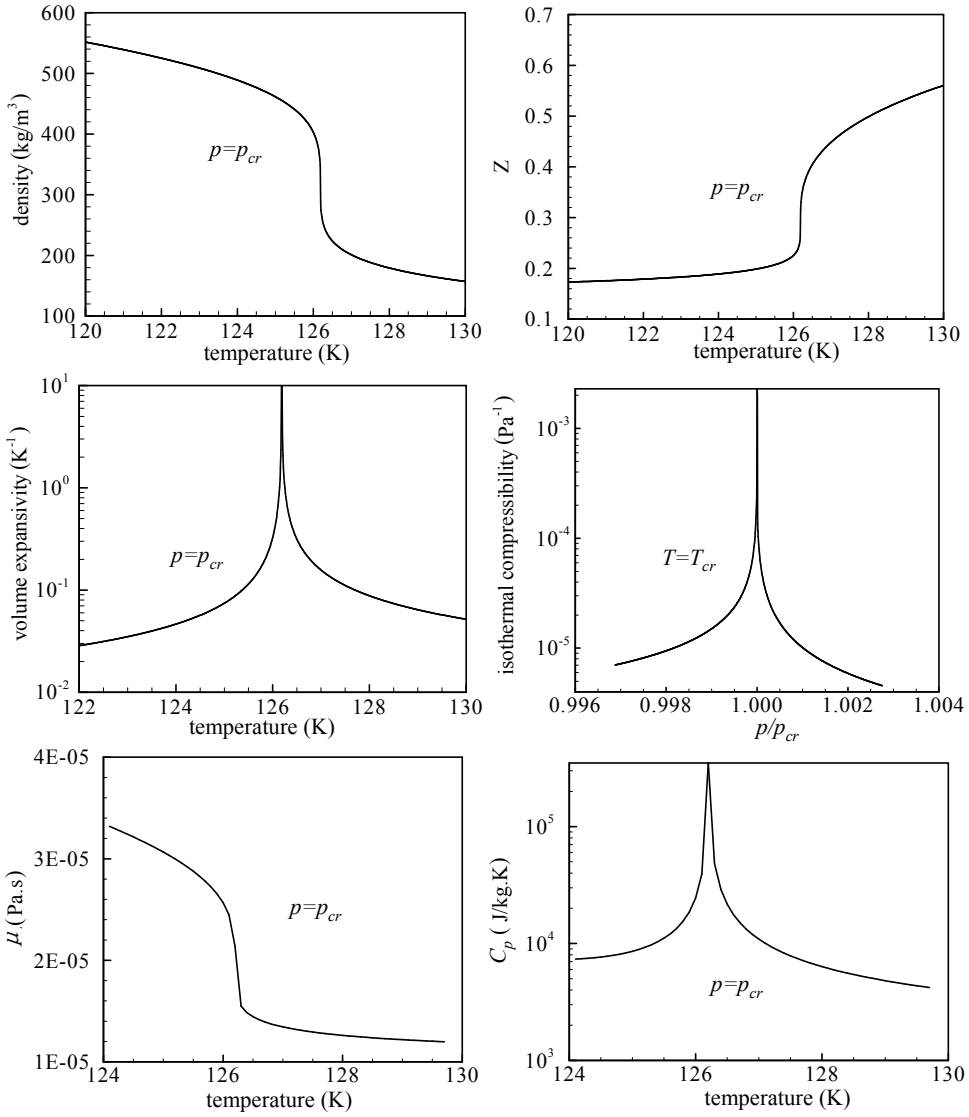

Figure 3: Thermodynamic and transport properties of nitrogen in the close vicinity of critical point (Z, μ and C_p are compressibility factor, dynamic viscosity and specific heat under constant pressure, respectively).

The physical model studied consists of one infinite vertical plane wall and infinite large region filled with near-critical nitrogen on the right side of the wall. The initial pressure is critical pressure of nitrogen ($p_0 = p_{cr}$) and the initial temperature is 0.1K above the critical temperature of nitrogen ($T_0 = T_{cr} + 0.1$K), where $p_{cr} = 3.4$Mpa, $T_{cr} = 126.2$K. The wall temperature T_w starts to increase linearly with time from the beginning ($t = 0$),

$$T_w(t) = T_0 + 5t. \tag{5.5}$$

The x axis is normal to the wall and directs from the wall to the fluid. The computa-

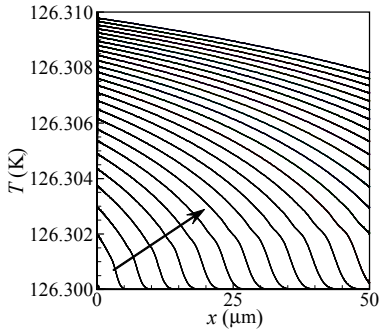

Figure 4: Temperature field evolution of side heated near-critical nitrogen from the beginning with an interval 0.015μs (the arrow indicates the direction of time evolution).

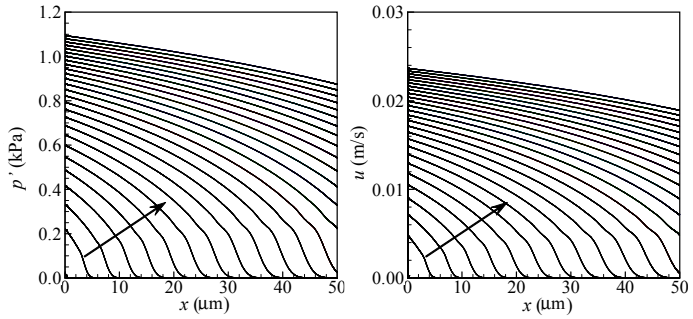

Figure 5: Propagation of the compression wave in side heated near-critical nitrogen from the beginning with an interval 0.015μs: gauge pressure (left) and velocity (right) (the arrow indicates the direction of time evolution).

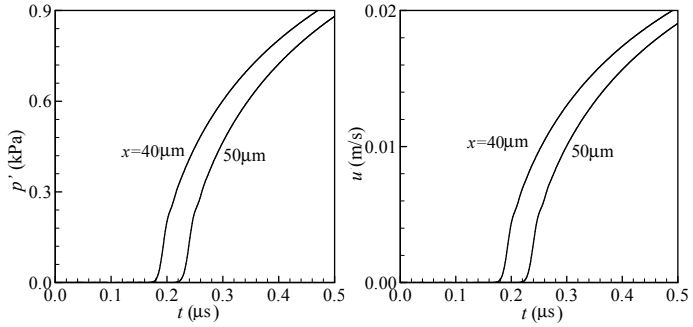

Figure 6: Propagation of the compression wave recorded by probes at $x = 40\mu$m and outflow boundary $x = 50\mu$m: gauge pressure (left) and velocity (right).

tional domain starts from the wall at $x = 0$ and ends in the nitrogen field at $x = 50\mu$m. Non-reflecting MOC boundary condition is used on the right side for the open boundary resultant from physical domain truncation.

The piston effect, another heating mechanism other than thermal diffusion and convection, is illustrated in Fig. 4. The entire field nitrogen was heated within one acoustic time period. Fig. 5 disclosures the origination of the fast heating mechanism, the strong compressive wave induced by wall boundary heating. The wave trans-

mitted right-towards and heated the fluid behind the wave front. Accurate and consistent boundary conditions must be implemented to avoid disturbance on the open boundary. Fig. 6 shows the local wave propagation process recorded at two sampling locations at $x = 40\mu$m and the open boundary ($x = 50\mu$m). The strong compressive wave passed through the open boundary transparently without any disturbance. This demonstrates that the current boundary condition method works well even for the near-critical fluid with anomalies shown in thermodynamic and transport properties.

5.3 Two-dimensional single vortex convection in real-fluid mixture

Characteristic boundary conditions are theoretically exact only for one-dimensional problems. To test the performance of the present method in multi-dimensional simulations, two-dimensional single vortex convection in a high-pressure cryogenic nitrogen/oxygen mixture with strong real-fluid effects is simulated. Similar to Poinsot and Lele's work [4], the vortex is given as follows. The stream function is

$$\psi = C \exp\Big(- \frac{x^2 + y^2}{2R^2} \Big). \tag{5.6}$$

The velocity distribution is

$$u = u_0 + \frac{\partial \psi}{\partial y}, \qquad v = -\frac{\partial \psi}{\partial x}. \tag{5.7}$$

The pressure distribution is

$$p = p_\infty + p' = p_\infty + p_\infty \big[(u - u_0)^2 + v^2 \big]^{\frac{1}{2}}. \tag{5.8}$$

The temperature is

$$T = T_0. \tag{5.9}$$

The mass fractions are

$$Y_{O_2} = 0.33, \qquad Y_{N_2} = 0.67. \tag{5.10}$$

The Mach number of free stream is

$$Ma = \frac{u_0}{a_0}. \tag{5.11}$$

The parameter C taking value of 5×10^{-3} determines the vortex strength. R equaling to one tenth of computational domain length is the characteristic radius of the vortex. u_0 is the mean flow velocity with different values for different Mach numbers. To test the current method for real fluids, the free stream temperature T_0 is set to 120K and the pressure P_∞ is set to 100atm. Under these conditions the compressibility factor Z of the nitrogen/oxygen mixture is 0.4, which is considerably far away from ideal gas. Both subsonic and supersonic cases are tested. For subsonic cases, both low Mach number case ($Ma = 0.1$) and moderate Mach number case ($Ma = 0.6$) are

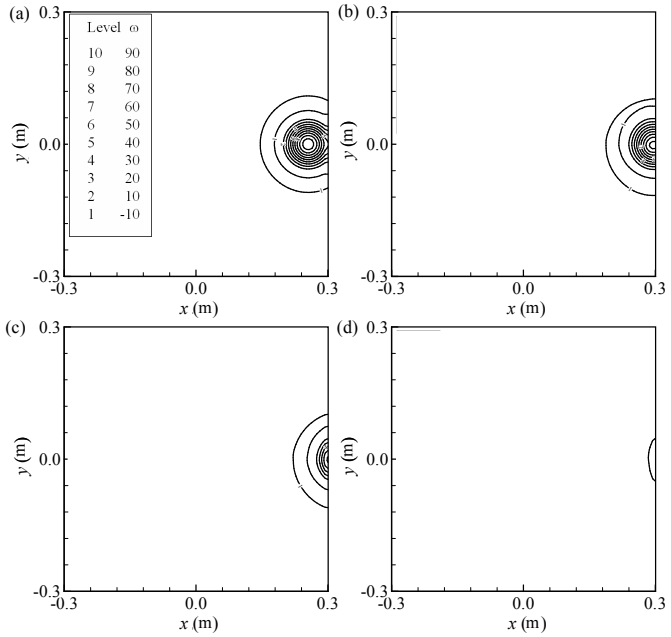

Figure 7: Evolution of vorticity field (s^{-1}) of a single vortex passing through the outflow boundary on the right-side, $Ma = 0.1$: (a) $t = 0.0$ms, (b) $t = 0.75$ms, (c) $t = 1.35$ms, (d) $t = 2.5$ms.

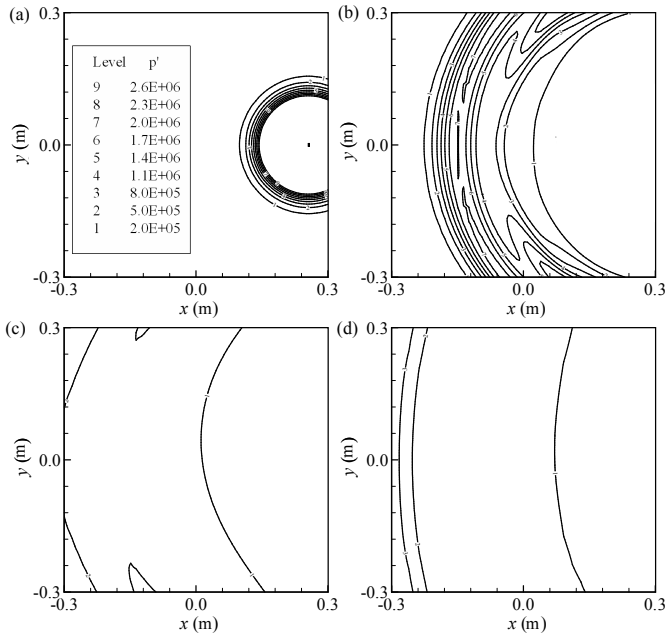

Figure 8: Evolution of gauge pressure field (Pa) of a single vortex passing through the outflow boundary on the right-side, $Ma = 0.1$: (a) $t = 0.0$ms, (b) $t = 0.75$ms, (c) $t = 1.35$ms, (d) $t = 2.5$ms.

tested. For the supersonic case $Ma = 1.6$ was applied. Fig. 7 shows the process of the single vortex transmitting through the outflow boundary in a uniform mean flow

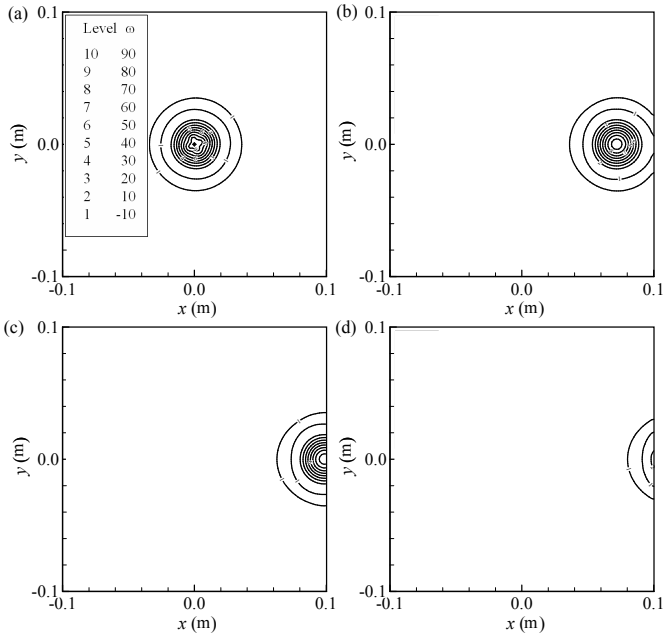

Figure 9: Evolution of vorticity field (s^{-1}) of a single vortex passing through the outflow boundary on the right-side, $Ma = 0.6$: (a) $t = 0.0$ms, (b) $t = 0.2$ms, (c) $t = 0.28$ms, (d) $t = 0.33$ms.

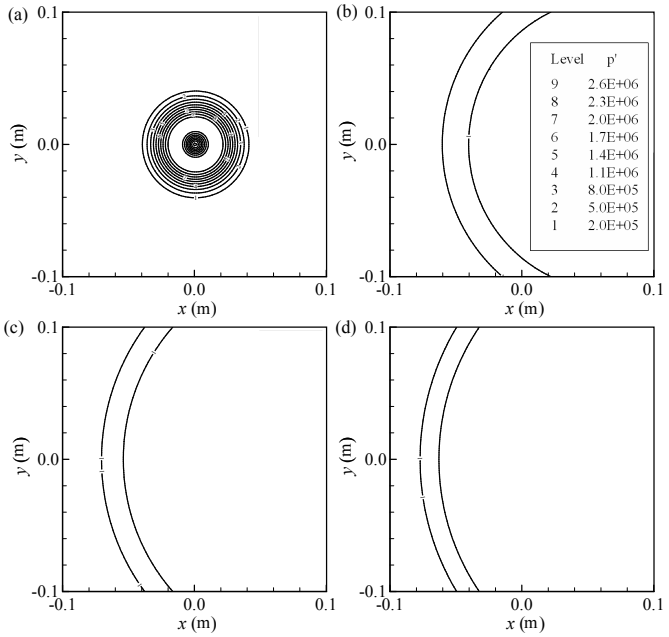

Figure 10: Evolution of gauge pressure field (Pa) of a single vortex passing through the outflow boundary on the right-side, $Ma = 0.6$: (a) $t = 0.0$ms, (b) $t = 0.2$ms, (c) $t = 0.28$ms, (d) $t = 0.33$ms.

with Mach number 0.1. Since viscosity is neglected in this case, the vortex keeps its original shape as at the beginning in the whole process and no diffusion happens. The

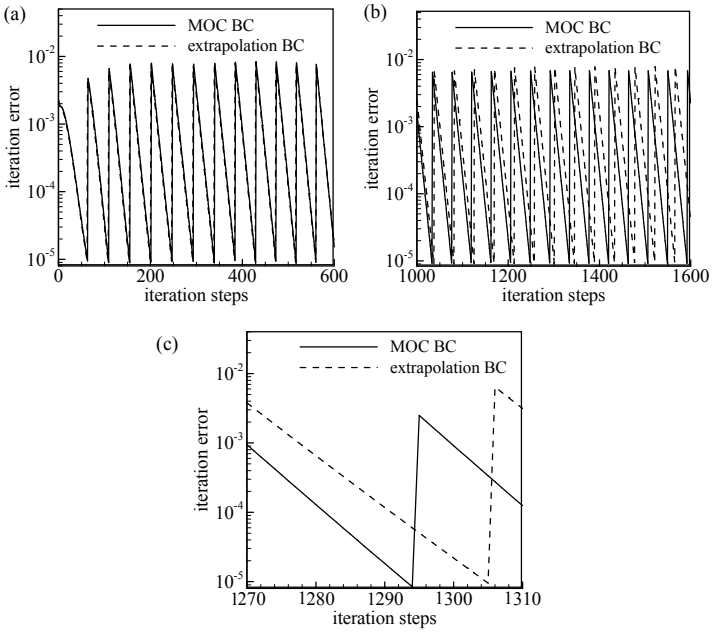

Figure 11: Comparison of convergence history of pseudo-time iteration in vortex convection case with $Ma = 0.6$ between current boundary condition method and simple extrapolation boundary method: (a) the early stage with uniform flow field, (b) the stage when the vortex passes through the outflow boundary, (c) zooming in of figure (b).

vortex passes through the boundary without distortion or reflection. Fig. 8 shows the process of the pressure field evolution with time. Due to the pressure difference in the radical direction of the vortex, the pressure wave spread from the vortex center towards outside with almost sound speed. The current method allows the pressure wave pass through the boundary smoothly and transparently without distortion or reflection. Satisfying results are also obtained for the moderate Mach number case $(Ma = 0.6)$ as shown in Figs. 9-10 and for the supersonic case. This indicates that the present boundary conditions work well for multidimensional multi-species real-fluid flows at all speeds.

Fig. 11 shows the convergence history of pseudo-time iteration in the case with free stream Mach number equal to 0.6. Comparison was made between the MOC boundary conditions and simple extrapolation boundary conditions. At the beginning, the outflow boundary has only uniform flows passing by, and therefore the residual of both cases are almost the same as shown in Fig. 11(a). As the vortex gets closer to the boundary, different convergence history from two types of boundary conditions shows up. The extrapolation boundary condition case needs more iteration steps to converge to the same residual level as in MOC boundary condition case (see Fig. 11(b)). The reason is that hydrodynamic and pressure fields can not pass the boundary smoothly, and obvious distortion of the flow field occurs in the near region of the outflow boundary. The distorted flow field induces larger residual error, leading to more iteration steps and computational time. Fig. 11(c) shows that in the MOC

boundary condition case, the converging speed is faster than that of the extrapolation boundary condition case, which is indicated by larger slop of residual converging history curve. This demonstrates that the current boundary method improves the computational efficiency.

6 Concluding remarks

Consistent boundary conditions based on the method of characteristics have been developed for general fluid mixtures flow at all speeds. The formulation derivation accounts for real-fluid effects, and preconditioning process is introduced to deal with flows with very low Mach number. The derivation is complex but the results are simple and easy to apply. Test cases are carried out for a broad range of fluid state and Mach number. The results appear to be satisfactory; both acoustic wave and flow field can pass the boundary smoothly without unphysical reflection, distortion or oscillation near the boundary. The current method has also been demonstrated to improve the computational efficiency of the preconditioning scheme and work well within the entire range of thermodynamic and hydrodynamic states.

Appendix

The preconditioning matrix Γ is given by

$$\Gamma = \begin{pmatrix} \Theta & 0 & 0 & -\frac{A_T}{A_\rho} \\ \Theta u & \rho & 0 & -\frac{A_T u}{A_\rho} \\ \Theta v & 0 & \rho & -\frac{A_T v}{A_\rho} \\ \Theta h_t + \left(\sum_{i=1}^{N} Y_i \tilde{e}_i - e - \frac{p}{\rho}\right)\left(\frac{\partial \rho}{\partial p}\right)_{T,Y_i} & \rho u & \rho v & \rho B_T - \frac{A_T e_t}{A_\rho} \\ \Theta Y_1 & 0 & 0 & -\frac{A_T Y_1}{A_\rho} \\ \vdots & \vdots & \vdots & \vdots \\ \Theta Y_{N-1} & 0 & 0 & -\frac{A_T Y_{N-1}}{A_\rho} \end{pmatrix}$$

$$\begin{pmatrix} -\frac{A_{Y_1}}{A_\rho} & \cdots & -\frac{A_{Y_{N-1}}}{A_\rho} \\ -\frac{A_{Y_1} u}{A_\rho} & \cdots & -\frac{A_{Y_{N-1}} u}{A_\rho} \\ -\frac{A_{Y_1} v}{A_\rho} & \cdots & -\frac{A_{Y_{N-1}} v}{A_\rho} \\ \rho B_{Y_1} - \frac{A_{Y_1} e_t}{A_\rho} & \cdots & \rho B_{Y_{N-1}} - \frac{A_{Y_{N-1}} e_t}{A_\rho} \\ \rho - \frac{A_{Y_1} Y_1}{A_\rho} & \cdots & -\frac{A_{Y_{N-1}} Y_1}{A_\rho} \\ \vdots & \ddots & \vdots \\ -\frac{A_{Y_1} Y_{N-1}}{A_\rho} & \cdots & \rho - \frac{A_{Y_{N-1}} Y_{N-1}}{A_\rho} \end{pmatrix}.$$

The Jacobian matrix A is

$$A=\begin{pmatrix} u(\frac{\partial\rho}{\partial p})_{T,Y_i} & \rho & 0 & 0 & -u\frac{A_T}{A_\rho} \\ 1+u^2(\frac{\partial\rho}{\partial p})_{T,Y_i} & 2\rho u & 0 & 0 & -u^2\frac{A_T}{A_\rho} \\ uv(\frac{\partial\rho}{\partial p})_{T,Y_i} & \rho v & \rho u & 0 & -uv\frac{A_T}{A_\rho} \\ uw(\frac{\partial\rho}{\partial p})_{T,Y_i} & \rho w & 0 & \rho u & -uw\frac{A_T}{A_\rho} \\ u[h_t+(\sum_{i=1}^{N}Y_i\widehat{e}_i-e-\frac{p}{\rho})+1](\frac{\partial\rho}{\partial p})_{T,Y_i} & h_t+\rho u^2 & \rho uv & \rho uw & u(\rho B_T-\frac{A_T e_t}{A_\rho}) \\ uY_1(\frac{\partial\rho}{\partial p})_{T,Y_i} & \rho Y_1 & 0 & 0 & -u\frac{A_T Y_1}{A_\rho} \\ \vdots & \vdots & \vdots & \vdots & \vdots \\ uY_{N-1}(\frac{\partial\rho}{\partial p})_{T,Y_i} & \rho Y_{N-1} & 0 & 0 & -u\frac{A_T Y_{N-1}}{A_\rho} \end{pmatrix}$$

$$\begin{pmatrix} -u\frac{A_{Y_1}}{A_\rho} & \cdots & -u\frac{A_{Y_{N-1}}}{A_\rho} \\ -u^2\frac{A_{Y_1}}{A_\rho} & \cdots & -u^2\frac{A_{Y_{N-1}}}{A_\rho} \\ -uv\frac{A_{Y_1}}{A_\rho} & \cdots & -uv\frac{A_{Y_{N-1}}}{A_\rho} \\ -uw\frac{A_{Y_1}}{A_\rho} & \cdots & -uw\frac{A_{Y_{N-1}}}{A_\rho} \\ u(\rho B_{Y_1}-\frac{A_{Y_1}e_t}{A_\rho}) & \cdots & u(\rho B_{Y_{N-1}}-\frac{A_{Y_{N-1}}e_t}{A_\rho}) \\ u(\rho-\frac{A_{Y_1}Y_1}{A_\rho}) & \cdots & -u\frac{A_{Y_{N-1}}Y_1}{A_\rho} \\ \vdots & \ddots & \vdots \\ -u\frac{A_{Y_1}Y_{N-1}}{A_\rho} & \cdots & u(\rho-\frac{A_{Y_{N-1}}Y_{N-1}}{A_\rho}) \end{pmatrix}.$$

Acknowledgments

The authors would like to thank Professor H. Ding for improving the manuscript. This work was supported in part by the National Natural Science Foundation of China (Nos. 11132010 and 11072236).

References

[1] T. COLONIUS, *Modeling artificial boundary conditions for compressible flow*, Ann. Rev. Fluid. Mech., 36 (2004), pp. 315–345.
[2] G. W. HEDSTROM, *Nonreflecting boundary conditions for nonlinear hyperbolic systems*, J. Comput. Phys., 30 (1979), pp. 222–237.
[3] K. W. THOMPSON, *Time-dependent boundary conditions for hyperbolic systems*, J. Comput. Phys., 89 (1987), pp. 439–461.
[4] T. J. POINSOT AND S. K. LELE, *Boundary conditions for direct simulations of compressible viscous flows*, J. Comput. Phys., 101 (1992), pp. 104–129.
[5] M. BAUM, T. POINSOT AND D. THEVENIN, *Accurate boundary conditions for multicomponent reactive flows*, J. Comput. Phys., 116 (1994), pp. 247–261.

[6] H. MENG AND V. YANG, *A unified treatment of general fluid thermodynamics and its application to a preconditioning scheme*, J. Comput. Phys., 189 (2001), pp. 277–304.
[7] B. ZAPPOLI AND D. BAILLY, *Anomalous heat transport by the piston effect in supercritical fluids under zero gravity*, Phys. Rev. A., 41 (1990), pp. 2264–2267.
[8] N. OKONG'O AND J. BELLAN, *Consistent boundary conditions for multicomponent real gas mixtures based on characteristic waves*, J. Comput. Phys., 176 (2002), pp. 330–344.
[9] Y. H. CHOI AND C. L. MERKLE, *The application of preconditioning in viscous flows*, J. Comput. Phys., 105 (1993), pp. 207–223.
[10] S. Y. HSIEH AND V. YANG, *A preconditioned flux-differencing scheme for chemically reacting flows at all Mach numbers*, Int. J. Comput. Fluid. Dyn., 8 (1997), pp. 31–49.
[11] N. ZONG AND V. YANG, *An efficient preconditioning scheme for real fluid mixtures using primitive pressure-temperature variables*, Int. J. Comput. Fluid. Dyn., 21 (2007), pp. 217–230.
[12] P. E. O. BUELOW, Convergence Enhancement of Euler and Navier-Stokes Algorithms, Ph.D thesis, The Pennsylvania State University, 1995.
[13] S. VENKATESWARAN AND C. L. MERKEL, *Dual time stepping and preconditioning for unsteady computations*, AIAA Paper, No. 95-0078, 1995.
[14] J. C. OEFELEIN AND V. YANG, *Modeling high-pressure mixing and combustion processes in liquid rocket engines*, J. Propul. Power., 14 (1998), pp. 843–857.
[15] J. C. OEFELEIN, *Mixing and combustion of cryogenic oxygen-hydrogen shear-coaxial jet flames at supercritical pressure*, Combust. Sci. Tech., 178 (2006), pp. 229–252.
[16] D. H. RUDY AND J. C. STRIKWERDA, *A nonreflecting outflow boundary condition for subsonic Navier-Stokes calculations*, J. Comput. Phys., 18 (1980), pp. 55–70.
[17] J. S. SHUEN, K. H. CHEN AND Y. H. CHOI, *A coupled implicit method for chemical nonequilibrium viscous flows at all speeds*, J. Comput. Phys., 106 (1993), pp. 306–318.
[18] A. JAMESON, *The evolution of computational methods in aerodynamics*, J. Appl. Math., 50 (1983), pp. 1052–1070.
[19] M. M. RAI AND S. CHAKRAVARTHY, *Conservative high-order accurate finite difference methods for curvilinear grids*, AIAA Paper, No. 1993-3380.
[20] P. JORGENSON AND E. TURKEL, *Central difference TVD schemes for time dependent and steady state problems*, J. Comput. Phys., 107 (1993), pp. 297–308.
[21] R. C. SWANSON AND E. TURKEL, *On central difference and upwind schemes*, J. Comput. Phys., 101 (1992), pp. 292–306.
[22] G. SOAVE, *Equilibrium constants from a modified Redlich-Kwong equation of state*, Chem. Eng. Sci., 27 (1972), pp. 1197–1203.
[23] R. T. JACOBSEN AND R. B. STEWART, *Thermodynamic of nitrogen including and vapor phase from 63K to 2000K with pressure to 10000 bar*, J. Phys. Chem. Ref. Data., 2 (1973), pp. 757–922.